Passive and active plasma deceleration for the compact disposal of electron beams

A. Bonatto, C. B. Schroeder, J.-L. Vay, C. G. R. Geddes, C. Benedetti, E. Esarey, and W. P. Leemans

---

Articles you may be interested in

Simulation study of a passive plasma beam dump using varying plasma density
Physics of Plasmas **24**, 023120 (2017); 10.1063/1.4977449

Efficient modeling of laser-plasma accelerator staging experiments using INF&RNO
AIP Conference Proceedings **1812**, 050005 (2017); 10.1063/1.4975866

Staging of laser-plasma accelerators
Physics of Plasmas **23**, 056705 (2016); 10.1063/1.4948280

Generation and pointing stabilization of multi-GeV electron beams from a laser plasma accelerator driven in a pre-formed plasma waveguide
Physics of Plasmas **22**, 056703 (2015); 10.1063/1.4919278

Control of quasi-monoenergetic electron beams from laser-plasma accelerators
AIP Conference Proceedings **1812**, 040005 (2017); 10.1063/1.4975852

Transport and phase-space manipulation of laser-plasma accelerated electron beams using active plasma lenses
AIP Conference Proceedings **1812**, 040006 (2017); 10.1063/1.4975853

Passive and active plasma deceleration for the compact disposal of electron beams

A. Bonatto,[1,2,a)] C. B. Schroeder,[1] J.-L. Vay,[1] C. G. R. Geddes,[1] C. Benedetti,[1] E. Esarey,[1] and W. P. Leemans[1]

[1]*Lawrence Berkeley National Laboratory, Berkeley, California 94720, USA*
[2]*CAPES Foundation, Ministry of Education of Brazil, Brasília, DF 700040-020, Brazil*

Plasma-based decelerating schemes are investigated as compact alternatives for the disposal of high-energy beams (beam dumps). Analytical solutions for the energy loss of electron beams propagating in passive and active (laser-driven) schemes are derived. These solutions, along with numerical modeling, are used to investigate the evolution of the electron distribution, including energy chirp and total beam energy. In the active beam dump scheme, a laser-driver allows a more homogeneous beam energy extraction and drastically reduces the energy chirp observed in the passive scheme. These concepts could benefit applications requiring overall compactness, such as transportable light sources, or facilities operating at high beam power. © *2015 AIP Publishing LLC*. [http://dx.doi.org/10.1063/1.4928379]

I. INTRODUCTION

Laser-driven plasma-based accelerators (LPAs) provide a compact way to produce high-energy electron beams.[1–3] Although LPAs sustain ultrahigh accelerating gradients, the compactness of the overall accelerator system may be limited by other components. The size of the laser system is a common consideration. In addition, high-energy beams require large and heavy beam dumps if conventional techniques are used for the disposal of the beams. A plasma-based decelerating stage may greatly reduce the required size of the beam dump by extracting the beam energy before disposal.

Two methods of plasma-based beam dumps are considered: passive and active. These methods rely on excitation of electron plasma waves to extract energy from a relativistic electron beam. In the passive beam dump, an energetic electron beam propagates in an initially quiescent plasma, exciting a wakefield. This scenario, usually investigated as a scheme to accelerate a second witness beam,[4–6] is approached here from the perspective of the energy that the driver loses to the wake along the propagation. In the active scheme, the beam propagates in the wake of a laser pulse, experiencing a net wakefield that is a superposition of the self-excited and laser-driven wakefields.

In a previous work,[7] 2D simulations in a slab geometry are presented indicating that a passive beam dump could reduce by orders of magnitude in distance required to decelerate a beam, in comparison to a material beam dump. Another advantage of the passive scheme over a material one is that high-energy radiation is not produced, since the deceleration is achieved by collective fields rather than by scattering. This greatly reduces the radioactivation hazard in the passive beam dump in comparison to a conventional one. However, due to the head to tail variation of the beam-driven wakefield, the beam energy is strongly chirped after the deceleration. As a consequence, particles near the head of the beam preserve most of their initial energy along the entire propagation in the plasma decelerating stage.

In an active beam dump scheme, by properly choosing the laser-plasma parameters and the initial phase relative to the beam, in principle, it is possible to flatten the net wakefield along the beam, in order to obtain a more homogeneous energy extraction. A laser-driven active plasma lens has been previously proposed.[8] Here, we consider a laser-driven active beam dump. The active scheme can also provide faster deceleration—with the same efficacy obtained for acceleration in an LPA—if compared to the passive one, since the total wakefield can be more intense than the beam-driven wakefield. A few cases of the active scheme have been investigated illustrating the potential advantage.[9,10] However, decelerating the beam to low energies requires further work to balance the laser and beam induced wakes and realize homogeneous energy extraction across the beam.

In this work, we derive analytical solutions for the evolution of the total energy of relativistic electron beams propagating in passive and active beam dumps. These solutions provide insight into the beam total energy loss in both schemes. In addition to these solutions, we perform particle-in-cell (PIC) simulations that allow us to assess the analytical solutions and to extend the analysis to non-relativistic regimes, where the analytical solutions are no longer valid. The simulations are performed first in 1D, to study the basic features of the beam deceleration, then in 2D axi-symmetric and in 3D, to incorporate the effects of the transverse dynamics in the beam total energy loss. As is shown in this paper, an active beam dump can decelerate electron beams with $\sim$ GeV energies to non-relativistic velocities after a few centimeters of propagation in the plasma, with a small, residual energy chirp.

This paper is organized as follows. In Sec. II, we derive a model to calculate the energy evolution of a high-energy

a)Electronic mail: abonatto@lbl.gov

electron beam propagating in a plasma, as a function of the beam-driven and laser-driven wakes acting on it. In Sec. III, we investigate the use of a passive plasma-based beam dump and derive an expression for the energy loss in this case. The active dumping scheme, including combination of laser and beam wake effects, is studied in Sec. IV. Estimates for the heating and radiation caused by plasma-based beam dumps are presented in Sec. V. A summary and conclusions are presented in Sec. VI.

II. THE MODEL

A. Beam energy loss

We consider a high-energy electron beam, with initial velocity close to the speed of light in vacuum, $v_z \simeq c$, propagating in a plasma treated as a cold-fluid of electrons with density n_0, in a fixed ionic neutralizing background. The beam is assumed to have cylindrical symmetry, with a profile given by $n_b(\zeta, r, s)$, where $\zeta \equiv z - ct$ is the coordinate in the co-moving frame, r the radial, transverse coordinate, and $s \equiv ct$ the propagation distance. Denoting by p_z and $p_\perp$, respectively, the longitudinal and transverse momentum from the beam particles, at $s = 0$ the beam has $p_z \simeq \gamma m_e c \gg p_\perp$, where m_e is the electron rest mass and γ is the relativistic factor. From the linearized equation of motion for the plasma response and Lorentz force, we have that the rate of energy change in the relativistic beam is

$$\frac{d\gamma}{ds} \simeq -k_p \frac{E_z}{E_0} = -k_p \left[\frac{E_{zb}}{E_0} + \frac{E_{z\ell}}{E_0} \right], \qquad (1)$$

where $k_p = \omega_p/c = (4\pi n_0 e^2/m_e c)^{1/2}$ is the plasma wave number, ω_p the electron plasma frequency, e the electron charge, E_{zb} is the beam self-driven longitudinal plasma wakefield, $E_{z\ell}$ is the laser-driven longitudinal plasma wakefield, and $E_0 = c m_e \omega_p/e$ the cold non-relativistic wave breaking electric field. We study two cases, passive ($E_{z\ell} = 0$) and active ($E_{z\ell} \neq 0$) dumping schemes (i.e., without and with a laser driver, respectively).

We consider a high initial energy for the beam, $\gamma \gg 1$, such that it is stiff and maintains its shape as it propagates in the plasma. Under this assumption, valid while the beam remains relativistic, the density profile of the beam does not depend on the propagation distance, namely, $n_b(\zeta, r, s) \simeq n_b(\zeta, r)$. As a consequence, the beam-driven wakefield does not change with s, $E_{zb} \simeq E_{zb}(\zeta, r)$. If a laser driver is present, phase slippage[2] between the beam ($v_z \simeq c$) and the laser (propagation velocity $\lesssim c$) can be an important effect and, hence, $E_{z\ell} = E_{z\ell}(\zeta, r, s, \psi_0)$, where ψ_0 determines the initial wake phase location of the beam with respect to the laser.

Assuming that the beam initial energy distribution is uniform and all the electrons have $\gamma(s = 0) = \gamma_0 \gg 1$, we can integrate Eq. (1) over the propagation distance s. We obtain the following expression for $\gamma(\zeta, r, s, \psi_0)$,

$$\gamma(\zeta, r, s, \psi_0) = \gamma_0 - k_p s [E_{zb}(\zeta, r)/E_0]$$
$$- k_p \int ds [E_{z\ell}(\zeta, r, s, \psi_0)/E_0]. \qquad (2)$$

In Eq. (2), the first term in the right-hand side is the initial energy, the second is the energy loss due to the beam-driven wakefield (passive beam dump)—which is linear in s and proportional to the amplitude of E_{zb} in every location (ζ, r) inside the beam—and the third term is the energy loss due to the laser-driven wakefield (active beam dump). The normalized total energy of the beam can be defined as $U(s, \psi_0) = \int_V dV \gamma(\zeta, r, s, \psi_0) n_b(\zeta, r)/n_0$. The initial value is $U(0, \psi_0) = U_0 = \gamma_0 \int_V dV \, n_b(\zeta, r)/n_0$. By using these definitions and $\gamma(\zeta, r, s, \psi_0)$, given in Eq. (2), we derive the following expression for the evolution of the normalized total beam energy,

$$\frac{U(s, \psi_0)}{U_0} = 1 - k_p s \frac{\int_V dV [E_{zb}(\zeta, r)/E_0][n_b(\zeta, r)/n_0]}{\gamma_0 \int_V dV \, n_b(\zeta, r)/n_0}$$
$$- k_p \frac{\int_0^s ds' \int_V dV [E_{z\ell}(\zeta, r, s', \psi_0)/E_0][n_b(\zeta, r)/n_0]}{\gamma_0 \int_V dV \, n_b(\zeta, r)/n_0}, \qquad (3)$$

which allows us to investigate the total energy loss of a beam propagating in either a passive or an active beam dumping scheme, once the beam and/or laser wakefields are specified. In order to study the energy chirp, which is relevant for shielding purposes, we evaluate the beam phase space distribution, obtained from PIC simulations.

B. Wakefield excitation

The excitation of wakefields driven either by electron beams or laser pulses in plasma-based accelerators is well-documented in the literature.[1,2,4,5,11] A plasma density perturbation $\delta n \equiv n - n_0$, excited by the space-charge force of a charged particle beam or by the ponderomotive force of an intense laser, gives rise to an axial electric field, E_z. If $\delta n/n_0 \ll 1$, and $E_z/E_0 \ll 1$, then the system is in the linear regime. Under these conditions, an electron beam with profile $n_b(\zeta, r)$ and/or a laser with normalized vector potential $\boldsymbol{a}(\zeta, r) \equiv eA(\zeta, r)/m_e c^2 < 1$ will excite a wake in the plasma that is described by the following equations, using the quasi-static approximation:[2]

$$\left(\frac{\partial^2}{\partial \zeta^2} + k_p^2 \right) \frac{\delta n}{n_0} = -k_p^2 \frac{n_b}{n_0} + \frac{1}{2} \nabla^2 a^2, \qquad (4)$$

$$\left(\nabla_\perp^2 - k_p^2 \right) \frac{E_z}{E_0} = -k_p \frac{\partial}{\partial \zeta} \frac{\delta n}{n_0} - k_p \frac{1}{2} \frac{\partial a^2}{\partial \zeta}. \qquad (5)$$

Equations (4) and (5) can be solved using the Green function to obtain analytical solutions for the wakefields.

1. Beam-driven wakefield

The solution for the beam-driven wake, $E_{zb}(\zeta, r)$, which can be obtained by solving Eqs. (4) and (5) with $a = 0$, is[2,11]

$$\frac{E_{zb}(\zeta, r)}{E_0} = -k_p^3 \int_\infty^\zeta d\zeta' \cos[k_p(\zeta - \zeta')]$$
$$\times \int_0^\infty dr' r' I_0(k_p r_<) K_0(k_p r_>) \, n_b(\zeta', r')/n_0, \qquad (6)$$

where I_0 and K_0 are the zeroth-order modified Bessel functions of the first and second kind, respectively, and $r_<(r_>)$ denotes the smaller (larger) of r and r', respectively. For example, for a beam with a half-sine longitudinal and parabolic transverse density profile, $n_b(\zeta, r)/n_0 = (n_b/n_0) \sin(\pi\zeta/L)(1 - r^2/r_b^2)$, if $0 \leq \zeta \leq L$ and $r \leq r_b$, or zero otherwise, Eq. (6) yields the following expression for the longitudinal wakefield:

$$\frac{E_{zb}(\zeta, r)}{E_0} = \frac{\pi k_p L (n_b/n_0)}{\pi^2 - k_p^2 L^2} \left\{ \cos\left[k_p(L - \xi)\right] - \cos\left(\frac{k_p \xi}{L}\right) \right\}$$
$$\times \left[1 - \frac{4 + k_p^2 r^2}{k_p^2 r_b^2} + 2I_0(k_p r)K_2(k_p r_b) \right], \quad (7)$$

for $0 \leq \zeta \leq L$ and $r \leq r_b$. In Sec. III, we will use Eqs. (3) and (6) to obtain analytical solutions for the beam total energy evolution in the passive case.

2. Laser-driven wakefield

Solving Eqs. (4) and (5) without a beam ($n_b = 0$) yields the following expression[2] for the laser-driven wakefield $E_{z\ell}(\zeta, r)$:

$$\frac{E_{z\ell}(\zeta, r, s)}{E_0} = -k_p^3 \int_\infty^\zeta d\zeta' \cos\left[k_p(\zeta - \zeta')\right] a^2(\zeta', r, s)/4, \quad (8)$$

with the linearly polarized laser envelope satisfying $a^2 \lesssim 1$. Equation (8) can be evaluated for a bi-Gaussian laser driver, with envelope given by $a^2(\zeta, r) = a_0^2 \exp(-\zeta^2/\sigma_\ell^2) \exp(-2r^2/r_w^2)$, where σ_ℓ and r_w are the laser length and waist, respectively. For small values of r, i.e., $r \ll r_w$, we may approximate the exponential transverse laser envelope by a parabolic one, $a^2(r) \sim \exp(-2r^2/r_w^2) \simeq 1 - 2r^2/r_w^2$. In the following, we assume that the laser pulse propagates in a preformed plasma channel, with laser waist and channel profile chosen to have the propagation quasi-matched,[12] such that the amplitude and width of the driven wakefield do not evolve.

Due to its high initial energy, the beam propagates faster than the laser in the plasma ($\gamma_0 \gg \gamma_g$, where γ_g is the relativistic factor associated to the laser group velocity v_g), and the phase slippage between the beam and laser is $\Delta\psi \sim k_p s(\beta_0 - \beta_g) \simeq k_p s/2\gamma_g^2$. We define the relative phase between the laser and the beam, ψ_0, such that, for $\psi_0 = 0$, the tail of the beam is positioned at $\zeta = 0$. Then, relativistic electrons contained in the region $0 \leq k_p\zeta \leq \pi/2$ of the wake will experience simultaneous axial decelerating and radial focusing forces; this is the optimum region in the active dumping scheme.

Considering the aforementioned conditions, we derive the following expression for the laser wakefield,

$$\frac{E_{z\ell}(\zeta, r, s, \psi_0)}{E_0} = \frac{E_{max}^{z\ell}}{E_0} \sin\left[k_p\zeta + \frac{k_p s}{2\gamma_g^2} + \psi_0\right]\left[1 - \frac{2r^2}{r_w^2}\right], \quad (9)$$

where $E_{max}^{z\ell}/E_0$ is the wake amplitude, $k_p s/2\gamma_g^2$ describes the phase slippage,[2] and ψ_0 is the initial phase between the beam

and the laser wake. Note that, for the given laser envelope, the value of $E_{max}^{z\ell}/E_0$ depends on the laser length σ_ℓ. For example, if $\sigma_\ell = \sqrt{2}/k_p$, then the laser pulse satisfies the linear resonance condition,[2] and the amplitude of the excited wake is $E_{max}^{z\ell}/E_0 \simeq 0.38\, a_0^2/(1 + a_0^2/2)^{1/2}$. In Sec. IV, Eqs. (3) and (9) will be used to obtain analytical solutions for the beam total energy evolution in the active case.

III. PASSIVE BEAM DUMP

In the passive dumping scheme, a highly relativistic electron beam propagates in an initially quiescent plasma, losing energy to the self-driven wakefield. We can investigate this process for a specific beam by inserting its profile $n_b(\zeta, r)$ in Eq. (6) to calculate the wakefield $E_{zb}(\zeta, l)$, and then from Eq. (3), obtaining an expression for the normalized beam energy $U(s)/U_0$. Since no laser is present, $E_{z\ell} = 0$ in Eq. (3) and the beam energy—while relativistic—is a linear function of the propagation distance s.

For a 1D flat-top beam for example, $n_b(\zeta)/n_0 = n_b/n_0$ for $-L \leq \zeta \leq 0$, and zero otherwise, the wakefield within the beam is $E_{zb}(\zeta)/E_0 = -(n_b/n_0)\sin(k_p\zeta)$, and the normalized total energy is

$$\frac{U(s)}{U_0} = 1 - s\frac{n_b}{n_0}\left[\frac{1 - \cos(k_p L)}{\gamma_0 L}\right]. \quad (10)$$

From Eq. (10), we see that the beam loses energy linearly with the propagation distance s, with a rate inversely proportional to the plasma density n_0 and beam energy γ_0. By setting $U(s)/U_0 = 0$ in Eq. (10), we calculate $s_{max} = \gamma_0 L/\{(n_b/n_0)[1 - \cos(k_p L)]\}$, which is the theoretical propagation distance at which the beam would lose all its energy. Note that this condition is never achieved: once the beam velocity is non-relativistic, the model is no longer valid. Also, as we shall discuss in this section, particles near the head of the beam preserve most of their initial energy along the entire propagation, preventing full beam energy depletion. However, s_{max} is a useful estimate of the length required to decelerate a beam in the passive beam dump scheme.

For a given set of parameters, the maximum rate of beam energy loss and, consequently, minimum deceleration length s_{max}, are achieved for $k_p L \simeq 2.33$. For example, in a plasma with $n_0 = 10^{18}\, \text{cm}^{-3}$, a 1D flat-top beam with $L \simeq 2.33/k_p \simeq 12.4\, \mu m$, $n_b/n_0 = 0.1$, and $\gamma_0 = 500$, has $s_{max} \simeq 3.7$ cm.

If we consider a 1D half-sine beam, with density profile given by $n_b(\zeta)/n_0 = (n_b/n_0)\sin(\pi\zeta/L)$ if $0 \leq \zeta \leq L$ and zero otherwise, we obtain the following expression for the evolution of the normalized beam total energy:[13]

$$\frac{U(s)}{U_0} = 1 - k_p s\frac{\pi^3 k_p L(n_b/n_0)\cos^2(k_p L/2)}{\gamma_0(\pi^2 - k_p^2 L^2)^2}. \quad (11)$$

The maximum rate of energy loss is $d(U/U_0)/ds|_{max} = -k_p(n_b/n_0)\pi^2/(16\gamma_0)$, for $k_p L \to \pi$. In this limit, $s_{max} = 16\gamma_0/[k_p(n_b/n_0)\pi^2]$. For example, in a plasma with $n_0 = 10^{18}\, \text{cm}^{-3}$, a 1D half-sine beam with $L \simeq \pi/k_p \simeq 16.7\, \mu m$, $n_b/n_0 = 0.1$, and $\gamma_0 = 500$, has $s_{max} \simeq 4.3$ cm.

In particular, for a half-sine beam density profile with length L, if the density is such that $k_p L \to \pi$, the beam fully occupies the first decelerating region of its self-driven wake, experiencing the maximum integrated electric field and total energy loss. For $k_p L > \pi$, the fraction of the length that exceeds the mentioned condition will be in an accelerating region of the wake, gaining energy.

In the following, we consider a half-sine longitudinal beam profile for both analytical and numerical solutions to be performed. From the perspective of the beam total energy loss, a half-sine profile exhibits a behavior similar to a Gaussian profile, and yet it provides simpler, more compact analytical solutions.

We complement these analytical results for the passive dumping scheme with PIC simulations, performed with the code Warp.[14] In particular, the energy loss observed in the simulation is compared to the analytical solution given in Eq. (11). Snapshots from the wakefield and phase space allow us to analyze the beam energy loss after the transition to non-relativistic regimes, where the assumptions adopted in the analytic solutions do not hold.

Typical LPA experimental setups[3] and previous numerical studies on plasma-based deceleration[9] report densities within the range of 10^{17}–10^{19} cm^{-3} and electron beams with normalized length $k_p L \lesssim 1$ and radius $k_p r_b \lesssim 1$. Since

plasma-based beam dumps could potentially be used in LPA applications, our parameters shall lie within these ranges. In particular, electrons with energy ~ 0.5 GeV ($\gamma \sim 1000$) are suitable for photon sources from LPA-based Thomson Scattering.[10] This energy gain/loss can be obtained before dephasing in a LPA with $n_0 \sim 10^{18}$ cm^{-3}.

For the simulation, we consider the same beam density profile, $n_b(\zeta)/n_0 = (n_b/n_0) \sin(\pi\zeta/L)$ if $0 \le \zeta \le L$ and zero otherwise, with $n_b/n_0 \simeq 0.315$, length $L \simeq 2.7\ \mu m$, and uniform initial energy distribution, $\gamma_0 = 1000$, propagating in an uniform plasma with density $n_0 = 10^{18}$ cm^{-3}. For these parameters, $k_p L \simeq 0.5 \lesssim 1$ and $E_z/E_0 \simeq 0.1 \ll 1$. Results are shown in Fig. 1. Figure 1(a) shows the spatial configuration of the beam (plotted as a red curve) and the wakefield $E_z/E_0 = E_{zb}/E_0$ at the beginning of the propagation ($s \simeq 0.7$ cm). Figure 1(b) shows the phase space, with $\gamma/\gamma_0 \simeq 1$ along the beam, for the same propagation distance. Although the total energy loss is a linear function of s, locally (at each longitudinal position), it depends on the amplitude of the electric field. Since the beam is short ($k_p L \le \pi/2$), E_z/E_0 rises from zero at the head ($k_p \zeta = 0$) to its maximum value along the beam at its tail. Due to this gradient, the tail becomes non-relativistic while the head still preserves most of its initial energy, causing the lengthening of the beam. Although the beam lengthening is not included
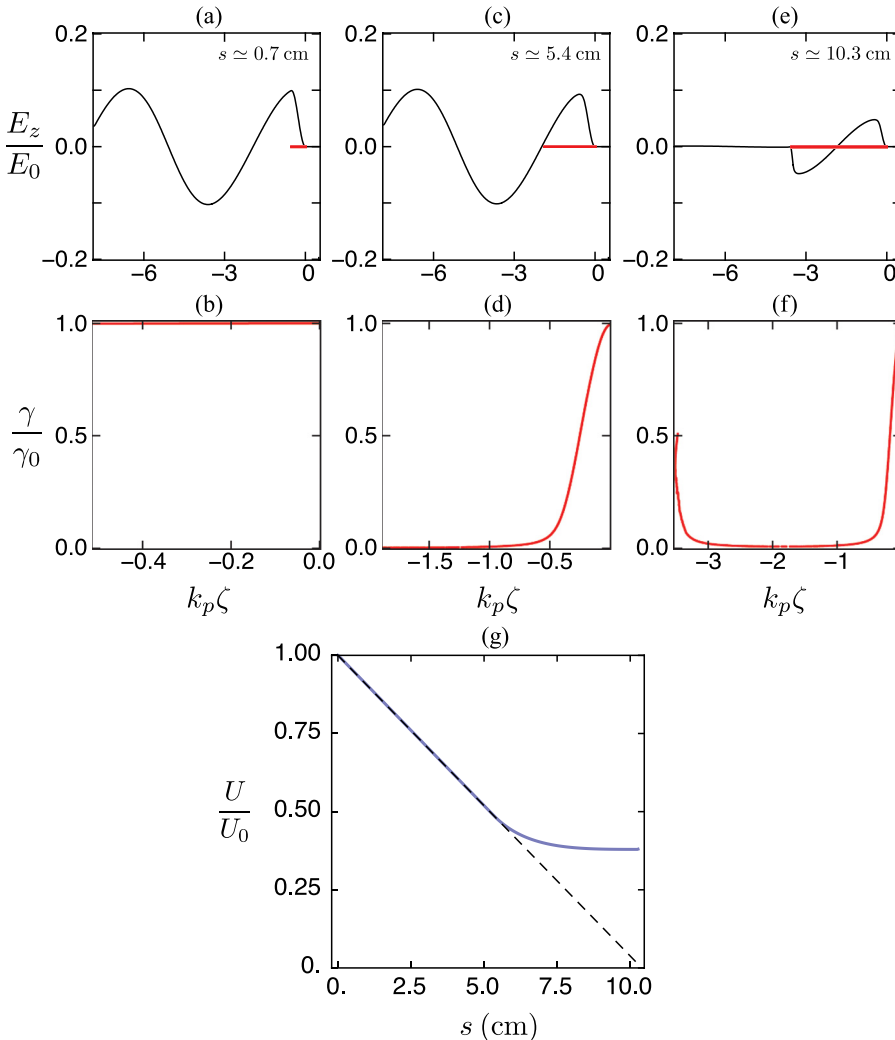

FIG. 1. Passive beam dump. 1D PIC simulation of an electron beam with peak density $n_b/n_0 \simeq 0.315$, length $L = 2.7\ \mu m$, and $\gamma_0 = 1000$, propagating in a plasma with density $n_0 = 10^{18}$ cm^{-3}. (a) Initial beam spatial distribution (red curve) and wakefield $E_z/E_0 = E_{zb}/E_0$ (black curve). (b) Phase space showing the normalized energy γ/γ_0 at $s \simeq 0.7$ cm. Due to the non-homogeneous deceleration, (c) the beam length increases, fully occupying the decelerating phase at $s = 5.4$ cm, and (d) the beam energy is chirped. (e) At $s \simeq 10.3$ cm, (e) the beam energy loss for particles closer to the head is nearly compensated by the energy gain for those closer to the tail. (f) At this propagated distance, some particles closer to the tail of the beam recovered approximately half of their initial energy. (g) Beam total energy evolution from the PIC simulation (blue curve) compared to the analytical solution (black, dashed curve). While the beam is relativistic ($\gamma/\gamma_0 \gg 1$), the total energy loss is linear with s and both solutions agree. After $s = 5.4$ cm, $\gamma/\gamma_0 \simeq 1$ and there is beam lengthening. Then, the agreement is broken, and the beam total energy loss saturates near $U/U_0 \simeq 0.38$.

in the analytical model, it can be investigated numerically. Figure 1(c) shows that at $s \simeq 5.4$ cm, the beam is approximately 4 times longer than at $s = 0$, reaching the accelerating phase, and Fig. 1(d) confirms that, when this happens, $\gamma/\gamma_0 \ll 1$ near the beam tail while $\gamma/\gamma_0 \sim 1$ at the head. Figs. 1(e) and 1(f) show that, after propagating $s \simeq 10.3$ cm, approximately half of the beam is gaining energy. At this point, Fig. 1(f) shows that the tail, initially formed by the particles that were decelerated to non-relativistic velocities, recovered half of its initial energy ($\gamma_{tail}/\gamma_0 \sim 0.5$).

In Fig. 1(g), we show the evolution of the total energy U/U_0 as the beam propagates through the passive dumping scheme. While the beam remains relativistic, it loses energy linearly and the PIC simulation result (solid curve, blue) agrees with the analytical solution from Eq. (11) (dashed curve, black). Once particles closer to the tail become non-relativistic ($\gamma/\gamma_0 \ll 1$), the assumption that the shape of the beam does not evolve is no longer valid. This explains why the energy loss from the PIC simulation departs from the analytical model after $s \simeq 5.4$ cm. For longer distances, the total energy remains approximately constant, $U/U_0 \simeq 0.38$. This plateau can be understood by examining Figs. 1(e) and 1(f): after $s \simeq 5.4$ cm, there is a balance between particles gaining (center-to-tail) and losing (center-to-head) energy. Previous 1D simulations[13] performed with another set of parameters show similar behavior.

So far, we considered a 1D example to investigate the basic features of a passive beam dump. In order to study the effects of the transverse dynamics in the energy loss, we include a parabolic profile with radius r_b in the half-sine 1D beam previously investigated.

Assuming the longitudinal half-sine and transverse parabolic profile, the beam density is given by $n_b(\zeta,r)/n_0 = (n_b/n_0) \sin(\pi\zeta/L)(1 - r^2/r_b^2)$ if $0 \le \zeta \le L$ and $r \le r_b$, or zero otherwise. With this azimuthally symmetric profile and Eqs. (3) and (6), we derive the analytical solution for the evolution of the beam energy,

$$\frac{U(s)}{U_0} = 1 - k_p s \, \frac{\pi^3 k_p L \, (n_b/n_0) \cos^2(k_p L/2)}{\gamma_0 (\pi^2 - k_p^2 L^2)^2}$$
$$\times \frac{2}{3} \left[\frac{k_p^2 r_b^2 - 6 + 24 \, I_2(k_p r_b) K_2(k_p r_b)}{k_p^2 r_b^2} \right], \quad (12)$$

where I_2 and K_2 are the second-order modified Bessel functions of the first and second kind, respectively. The limit $r_b \to \infty$ in Eq. (12) yields $U/U_0 = 1 - (2/3)(k_p s)[\pi^3 k_p L (n_b/n_0) \cos(k_p L/2)^2]/[\gamma_0(\pi^2 - k_p^2 L^2)^2]$, which is similar to the energy loss of a 1D half-sine beam, Eq. (11). The only difference—the factor of 2/3—is a geometric factor introduced by the chosen transverse beam profile. For a flat-top radial profile, this factor would be equal to 1, and we would recover exactly the energy loss of a 1D half-sine beam, Eq. (11).

To investigate the passive beam dumping in this geometry and check the validity of Eq. (12), we performed a 3D PIC simulation with Warp, using the Lorentz boosted frame modeling technique,[15] with $\gamma_{frame} = 12$. In the simulation, we used a uniform plasma with $n_0 = 10^{18}$ cm^{-3} and the same

beam profile used to derive Eq. (12), with the following parameters: $L = r_b \simeq 2.7 \, \mu$m ($k_p L = k_p r_b \simeq 0.5 \lesssim 1$), $n_b/n_0 \simeq 3$, $\gamma_0 = 1000$ and normalized RMS emittance $\epsilon_x = \epsilon_y \simeq 0.35 \, \mu$m rad ($k_p \epsilon_x = k_p \epsilon_y \simeq 0.07$), chosen to minimize the variation of the RMS beam radius. Note that, for these parameters, the choice of $n_b/n_0 \simeq 3$ corresponds to a charge of $Q \simeq -10$ pC, exciting a wake with the same amplitude used in the 1D case, $E_{zb}/E_0 \simeq 0.1$. Results, including a comparison with the energy loss calculated with Eq. (12), are shown in Fig. 2. Figure 2(a) shows the spatial configuration of the beam (plotted in green) and the wakefield $E_z/E_0 = E_{zb}/E_0$ after propagating $s \simeq 1.1$ cm in the plasma. Since both longitudinal and transverse wakes rise from zero at the beam's head, particles at this location do not experience decelerating or focusing forces, maintaining their initial trajectories along the propagation. This can be seen in Fig. 2(a), where the beam radius is expanding at the head, with a rate given by the initial transverse divergence, while its body undergoes betatron oscillations[2] in the focusing force of the wake. The phase space depicted in Fig. 2(b) shows particles closer to the tail—which are subjected to a stronger longitudinal wakefield—losing energy, while those closer to the head preserve it. Note that the longitudinal phase space plot of the 3D simulation shows a local energy spread at each position along the beam. Since the longitudinal wake is a function of the radial coordinate with a peak on-axis, the energy loss is smaller for particles off-axis, resulting in the local spread in energy. As the beam propagates, the tail is decelerated and the energy chirping increases. Then, when the tail becomes non-relativistic, the beam undergoes the same lengthening process observed in the 1D case. Figs. 2(c) and 2(d) show this behavior at $s \simeq 6.7$ cm. For longer propagation distances, particles at the tail are longitudinally accelerated and radially expelled after reaching accelerating and defocusing regions of the wake, respectively. This can be seen in Figs. 2(e) and 2(f), plotted at $s \simeq 14.5$ cm. For this propagation distance, some particles at the tail recovered approximately 75% of its initial energy ($\gamma_{tail}/\gamma_0 \simeq 0.75$).

The normalized beam energy, plotted in Fig. 2(g), depicts the same behavior seen in the 1D case: While the beam is relativistic, it loses energy in a linear way and the PIC simulation result (solid curve, blue) agrees with the analytical solution given in Eq. (12) (dashed curve, black). After $s \simeq 6$ cm, the tail starts to gain energy from the wake. When energy loss and gain nearly compensate, the total energy loss of the beam saturates at approximately $U/U_0 \simeq 0.43$.

Despite the higher energy spread in longitudinal phase space and the transverse ejection of particles (due to defocusing regions), the evolution of the normalized total energy in the passive dumping scheme observed in both 1D and 3D simulations is similar. The minimum energy achieved in both cases is close to $U/U_0 \simeq 0.4$.

In Fig. 3, we show s_{max} as a function of the plasma density and the initial energy of a beam with fixed length, radius, and charge. We obtain s_{max} by solving the equation $U(s_{max})/U_0 = 0$, where $U(s)/U_0$ is given Eq. (3) for the same beam profile and parameters adopted in the 3D PIC simulation, calculating $n_b/n_0 = -Q/(n_0 e \, r_b^2 L)$ and k_p self-consistently for each chosen value of n_0. For these
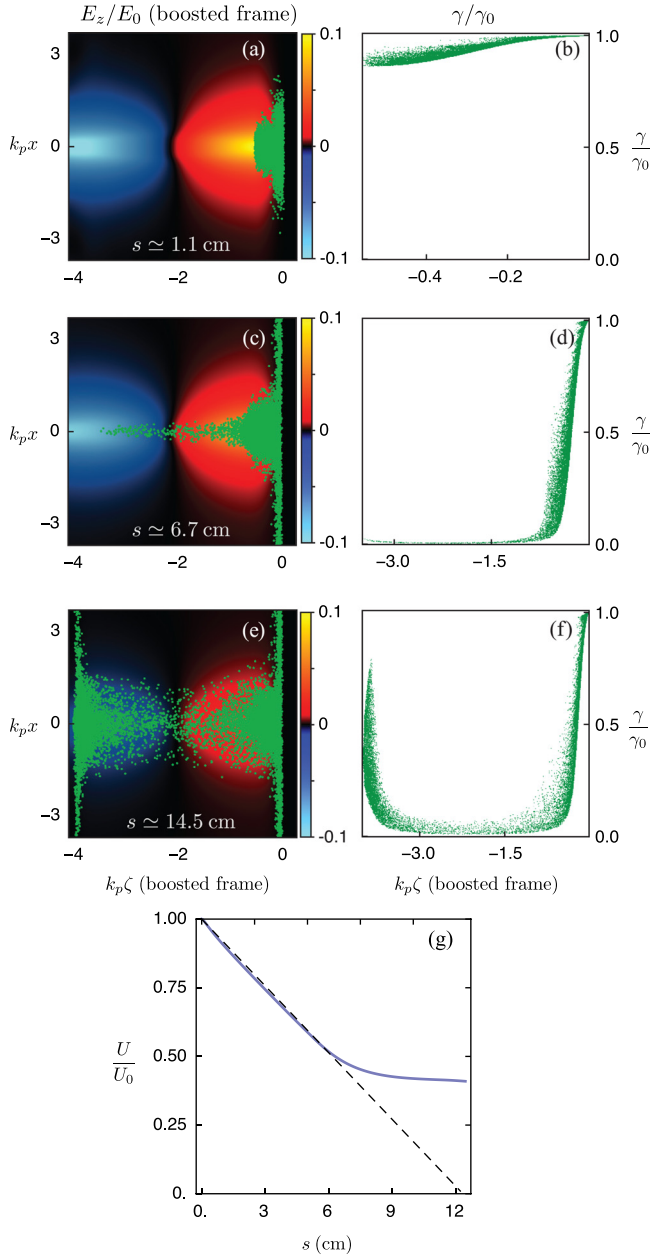
FIG. 2. Passive beam dump. 3D PIC simulation of an electron beam with peak density $n_b/n_0 \simeq 3$, length and radius $L = r_b = 2.7\,\mu m$ and initial energy $\gamma_0 = 1000$, propagating in a flat plasma with density $n_0 = 10^{18}\,cm^{-3}$. (a) Beam spatial distribution (green dots) and wakefield $E_z/E_0 = E_{zb}/E_0$ (color scale). At $s \simeq 1.1\,cm$, the beam radius shows some effects of betatron oscillations, and (b) the phase space is slightly chirped. At $s = 6.7\,cm$, due to the beam lengthening, (c) particles are longitudinally crossing the decelerating phase of the wake. Transversely, the beam radius keeps expanding at the head, with a rate given by its initial divergence. (d) At this distance, the phase space is strongly chirped. (e) At $s = 14.5\,cm$, after reaching accelerating and defocusing regions of the wake, respectively, particles closer to the tail of the beam are gaining energy and being radially expelled. (f) The phase space shows that, at this distance, some of these particles have $U/U_0 \simeq 0.75$. (g) Beam total energy evolution from the PIC simulation (blue curve) compared to the analytical solution (black, dashed curve). While the beam is relativistic ($\gamma/\gamma_0 \gg 1$). The beam total energy loss saturates near $U/U_0 \simeq 0.43$.

parameters, $s_{max} \simeq 12\,cm$ for a beam with $\gamma_0 = 1000$ propagating in a plasma with $n_0 = 10^{18}\,cm^{-3}$. This is the case plotted in Fig. 2(g), where the dashed curve representing the theoretical model reaches zero at $s \simeq 12\,cm$.
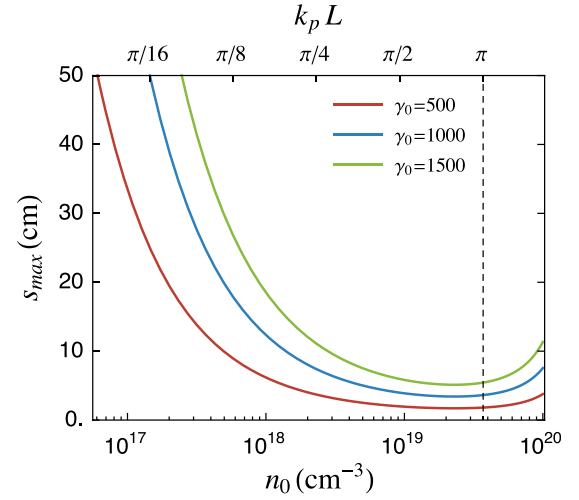

FIG. 3. Dependence of s_{max} on ζ, plasma density, n_0, and beam initial energy, γ_0, for a passive beam dump. The beam profile is given by $n_b(\zeta,r)/n_0 = (n_b/n_0)\sin(\pi\zeta/L)(1 - r^2/r_b^2)$, if $0 \le \zeta \le L$ and $r \le r_b$, or zero otherwise, with $n_b/n_0 = -Q/(n_0 e\, r_b^2 L)$, $L = r_b \simeq 2.7\,\mu m$, and charge $Q \simeq -10\,pC$. For a fixed beam length L, the higher the density, the longer k_pL is inside the decelerating region of the beam-driven wakefield, requiring a shorter distance s_{max} to be dumped. If $k_pL = \pi$, the energy loss is maximum and s_{max} is minimum. For $k_pL > \pi$, the beam is partially inside the accelerating region of the wake, causing s_{max} to grow again.

Since $k_p \propto n_0^{1/2}$, the normalized beam length k_pL increases as the density increases. While $k_pL < \pi$, the beam occupies a progressively longer fraction of the decelerating wake, increasing the rate of energy loss and, consequently, shortening s_{max}. When $k_pL = \pi$, the beam occupies the entire decelerating region of the wake. Then, the energy loss is maximum and s_{max} is minimum. As k_pL increases beyond π, an increasing fraction of the beam will be inside the accelerating region of the wake, gaining energy from it. For this reason, s_{max} increases for $k_pL > \pi$.

In previous works,[7,13] PIC simulations of passive beam dumps showed beam total energies within the range of $U/U_0 = 0.25 \sim 0.40$ after deceleration. Better results ($U/U_0 \sim 0.10$) were obtained by tailoring the plasma profile.[7] Even though, for all cases, the head of the beam preserved its initial energy along the propagation, these remaining high-energy particles still require large beam dumps for a safe radiation shielding. In Sec. IV, we discuss the active beam dump, where, instead of tailoring the plasma profile, a laser-driven wake is used to flatten the net wakefield acting over the beam. The active dump significantly reduces the energy chirp observed in the passive beam dump case, allowing higher energy extraction ($U/U_0 \lesssim 0.10$) in a shorter propagation distance.

IV. ACTIVE BEAM DUMP

The passive dumping scheme described in Sec. III can be improved by using a laser-driven wakefield to tailor the shape of the axial electric field experienced by the beam. In principle, depending on the laser parameters and injection phase, the net wakefield $E_z/E_0 = (E_{zb} + E_{z\ell})/E_0$ can be stronger and more homogeneous along the beam than E_{zb}/E_0 itself. In the active beam dump, an electric field with such

properties enables us to extract more energy from the beam, in a shorter distance, and with a lower energy spread if compared to the passive scheme.

To investigate the active beam dump scheme, we first consider a 1D half-sine beam, with a density profile given by $n_b(\zeta, r)/n_0 = (n_b/n_0) \sin(\pi\zeta/L)$ if $0 \leq \zeta \leq L$, or zero otherwise. We use this profile in Eq. (6) to calculate the beam-driven wakefield $E_{zb}(\zeta, l)$, and Eq. (9) in the limit $r_w \to \infty$ to obtain the 1D laser wake $E_{z\ell}(\zeta, s, \psi_0)$. Equation (3) can be used to obtain the normalized beam energy,

$$\frac{U(s, \psi_0)}{U_0} = 1 - k_p s \frac{\pi^3 k_p L \left(n_b/n_0\right) \cos^2\left(k_p L/2\right)}{\gamma_0 \left(\pi^2 - k_p^2 L^2\right)^2}$$
$$- \frac{4\pi^2 \gamma_g^2 \left(E_{max}^{z\ell}/E_0\right) \cos\left(k_p L/2\right)}{\gamma_0 \left(\pi^2 - k_p^2 L^2\right)}$$
$$\times \sin\left[\frac{k_p s}{4\gamma_g^2}\right] \sin\left[\frac{k_p L}{2} + \frac{k_p s}{4\gamma_g^2} + \psi_0\right]. \qquad (13)$$

The first and second terms on the right-hand side of Eq. (13) correspond to the initial normalized energy (which is 1 at $s = 0$) and the change in energy caused by the beam-driven wakefield, respectively. The last term of the right-hand-side of Eq. (13) takes into account the change in beam energy caused by the laser-driven wake.

The behavior of the basic features of the active beam dump have been investigated by means of 1D PIC simulations. We considered the beam-plasma parameters of Sec. III (a half-sine beam with $n_b/n_0 \simeq 0.315$, $L \simeq 2.7\,\mu m$, and $\gamma_0 = 1000$, in an uniform plasma with $n_0 = 10^{18}\,cm^{-3}$). To flatten the net axial electric field along the beam, we add a linearly polarized Gaussian laser pulse, with envelope given by $a^2(\zeta) = a_0^2 \exp(-\zeta^2/\sigma_\ell^2)$, $a_0 = 1$ (chosen to flatten the net axial electric field along the beam), and $\sigma_\ell = \sqrt{2}/k_p \simeq 7.5\,\mu m$. For these parameters, the wake amplitude is $E_{max}^{z\ell}/E_0 \simeq 0.31$). The laser wavelength is $\lambda_0 = 0.8\,\mu m$ and the group velocity of the laser corrected for its intensity[16] is $\gamma_g \simeq k_0/k_p(1 + 0.051a_0^2)$, where $k_0 = 2\pi/\lambda_0$. The initial phase between the beam and laser wake is $\psi_0 = 0$, i.e., the tail of the beam is aligned with the beginning of the decelerating phase of the wake. The evolution of the electric field and beam phase space, as well as the energy loss from the simulation compared to the analytical solution Eq. (13), is presented in Fig. 4. Figure 4(a), plotted at $s \simeq 0.01$ cm, shows the beam (red curve) and the net wakefield $E_z/E_0 = (E_{zb} + E_{z\ell})/E_0$ (black curve). With the chosen initial phase, the beam is placed at the beginning of a decelerating region of the laser wake. Figure 4(b) shows the initially flat phase space. Due to the deceleration, the phase slippage toward the laser pulse (initially strong because $\gamma_0 \gg \gamma_g$) is
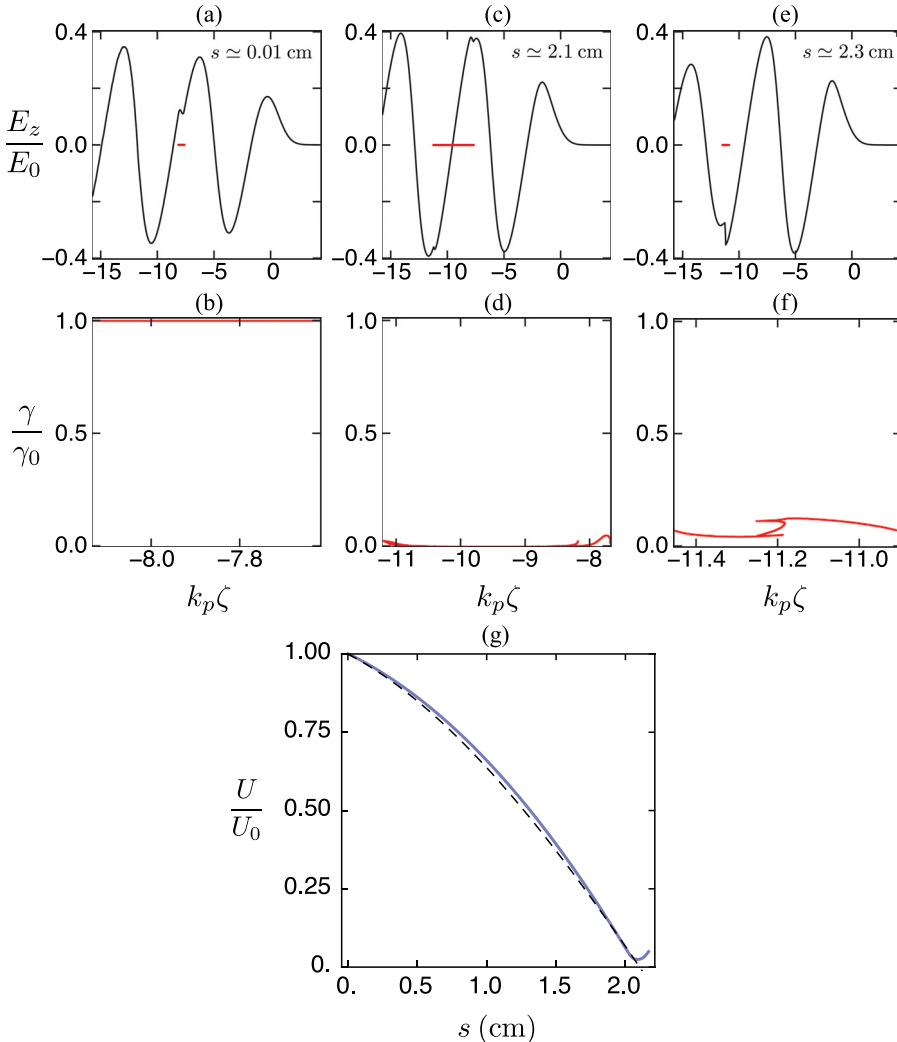

FIG. 4. Active beam dump. 1D PIC simulation of an electron beam with peak density $n_b/n_0 \simeq 0.315$, length $L = 2.7\,\mu m$ and initial energy $\gamma_0 = 1000$, propagating in a plasma with density $n_0 = 10^{18}\,cm^{-3}$. (a) Beam spatial distribution (red curve), net wakefield $E_z/E_0 = (E_{zb} + E_{z\ell})/E_0$ (black curve) and (b) initial phase space. (c) Beam distribution and (d) a near-flat phase space at $s \simeq 2.1$ cm, with $\gamma/\gamma_0 \ll 1$ across the beam. (e) At $s \simeq 2.3$ cm, the beam is in the accelerating phase of the wake, (f) gaining energy. (g) Analytical solution of the normalized total energy U/U_0 (dashed curve, black) compared to the PIC simulation result (solid curve, blue). After reaching the minimum value observed, $U/U_0 \simeq 0.028$ at $s \simeq 2.1$ cm, the beam gains energy from wakefield and is accelerated.

progressively reduced as the beam propagates and loses energy. Then, when $\gamma < \gamma_g$, the slippage direction is inverted and the beam slips backwards. Due to this effect and to the beam lengthening that occurs when it becomes partially non-relativistic, the beam reaches the accelerating region of E_z/E_0 and start gaining energy. This is shown in Fig. 4(c), plotted for $s \simeq 2.1$ cm, where energy reaches its minimum value $U/U_0 \simeq 0.024$. Figure 4(d) shows at $s \simeq 2.1$ cm an almost flat phase space profile, with $\gamma/\gamma_0 \ll 1$ along the beam from head to tail, resulting from the more homogeneous energy extraction in the active dumping scheme. Figs. 4(e) and 4(f), plotted at $s \simeq 2.3$ cm, show that, shortly after losing almost all its energy, the whole beam slips into the accelerating phase of the wake and starts gaining energy.

Even though the basic features of an active beam dump scheme can be studied in 1D, a 3D study is required to assess the role of transverse beam dynamics. We considered the wake generated by a bi-Gaussian laser driver, $a^2(\zeta, r) = a_0^2 \exp(-\zeta^2/\sigma_\ell^2) \exp(-2r^2/r_w^2)$, where the laser waist, r_w, is much larger than the electron beam radius, namely, $r_w \gg r_b$. As mentioned in Sec. II B 2, the amplitude and width of the laser (and thus the wake) do not evolve due to the quasi-matched propagation in a preformed plasma channel. Then, the use of Eqs. (3) and (6) for a beam with a half-sine longitudinal and parabolic transverse density profile, namely, $n_b(\zeta, r)/n_0 = (n_b/n_0) \sin(\pi\zeta/L)(1 - r^2/r_b^2)$ for $0 \leq \zeta \leq L$ and $r \leq r_b$, or zero otherwise, yields the following expression for the beam normalized energy:

$$
\begin{aligned}
\frac{U(s)}{U_0} &= 1 - k_p s \, \frac{\pi^3 k_p L \, (n_b/n_0) \cos^2\!\big(k_p L/2\big)}{\gamma_0 \big(\pi^2 - k_p^2 L^2\big)^2} \\
&\times \frac{2}{3}\left[1 + \frac{24\, I_2(k_p r_b) K_2(k_p r_b) - 6}{(k_p r_b)^2}\right] \\
&- \frac{4\pi^2 \gamma_g^2 \big(E_{max}^{z\ell}/E_0\big)\cos\big(k_p L/2\big)}{\gamma_0 \big(\pi^2 - k_p^2 L^2\big)}\left[1 - \frac{2}{3}\frac{r_b^2}{r_w^2}\right] \\
&\times \sin\!\left[\frac{k_p s}{4\gamma_g^2}\right] \sin\!\left[\frac{k_p L}{2} + \frac{k_p s}{4\gamma_g^2} + \psi_0\right].
\end{aligned}
\tag{14}
$$

To perform simulations for the active case, we use the code INF&RNO,[17,18] a 2D axi-symmetric PIC code. Simulations performed in this geometry reduce computational cost, while maintaining physical fidelity. We considered a linearly polarized bi-Gaussian laser pulse, with $\sigma_\ell = \sqrt{2}/k_p \simeq 7.5\,\mu$m, $r_w = \pi/k_p \simeq 17\,\mu$m, and $a_0 = 1$. The laser is matched in a parabolic plasma channel, with on-axis density $n_0 = 10^{18}$ cm^{-3}. The group velocity of the laser, taking into account contributions from plasma channel and plasma wave guiding,[16] is given by $\gamma_g = k_0/k_p(1 + 4/r_w^2)^{-1/2}$ $(1 + 0.051 a_0^2)$. With these parameters, the maximum amplitude of the laser-driven wake is $E_{max}^{z\ell} \simeq 0.31$. The beam parameters are $L = r_b \simeq 2.7\,\mu$m, $\gamma_0 = 1000$, $n_b/n_0 \simeq 3$, $\epsilon_x = \epsilon_y \simeq 0.35\,\mu$m rad, and $\psi_0 = 0$. Simulation results are presented in Fig. 5. Figure 5(a) shows the spatial configuration of the beam (green dots) and the net axial electric field $E_z/E_0 = (E_{zb} + E_{z\ell})/E_0$. The initial bunch phase is chosen to have the tail of the beam positioned at the beginning of a
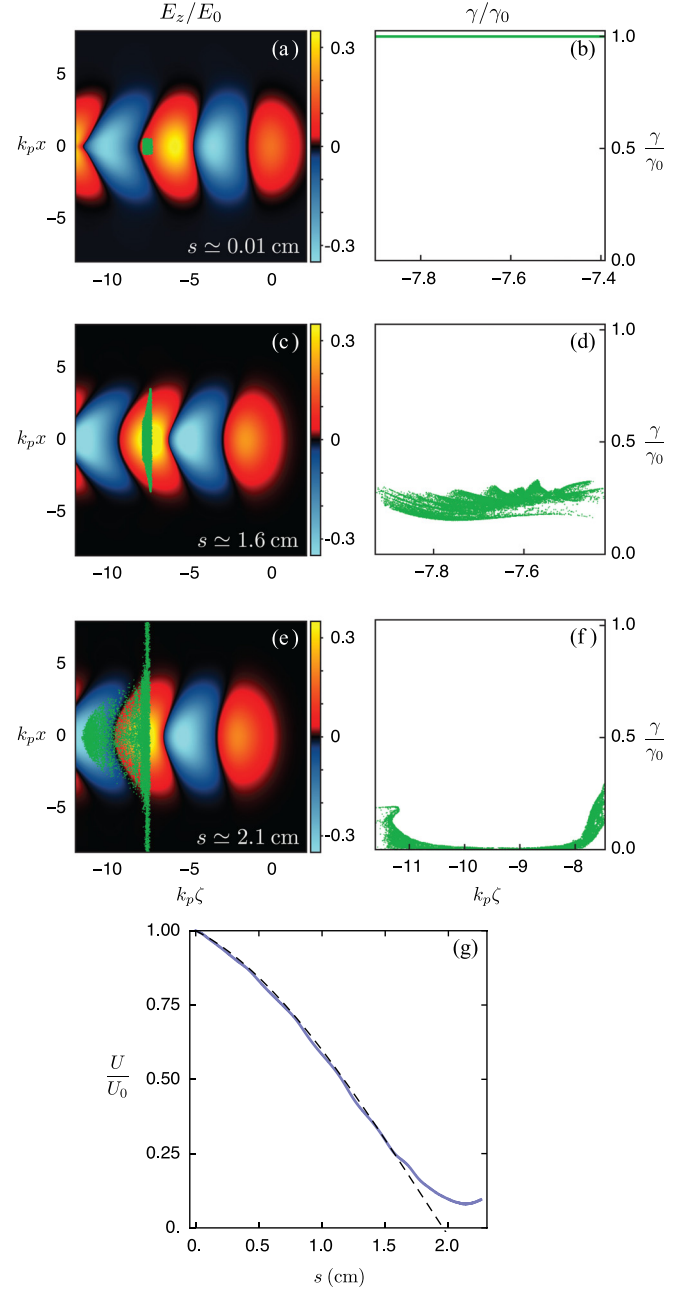

FIG. 5. Active beam dump. 2D axi-symmetric PIC simulation of an electron beam with peak density $n_b/n_0 \simeq 3$, length and radius $L = r_b = 2.7\,\mu$m and initial energy $\gamma_0 = 1000$, propagating in a plasma channel with density $n_0 = 10^{18}$ cm^{-3} on-axis. The laser-driven wake is excited by a Gaussian laser pulse, linearly polarized, with $a_0 = 1$. (a) Beam spatial distribution (green dots), net wakefield $E_z/E_0 = (E_{zb} + E_{z\ell})/E_0$ (color scale), and (b) initial phase space. At $s \simeq 1.6$ cm, (c) the beam radius is greater at the head than at the tail, due to the gradient of the focusing force. (d) The phase space is still approximately flat, although with some energy spread due to the betatron oscillations. (e) At $s \simeq 2.1$ cm, particles are being expelled at the head of the beam, which is in a defocusing region of the wake, and accelerated at its tail. (f) At this distance, the phase space shows that most of the beam energy was extracted with a small chirp if compared to the passive case. (g) Analytical solution of U/U_0 (dashed curve, black) compared to the PIC simulation result (solid curve, blue). The minimum beam total energy, $U \simeq 0.08$, was observed at $s \simeq 2.1$ cm.

longitudinally decelerating and transversely focusing region of the wake. Due to the fact that, for these laser-plasma parameters, only a quarter of the wake phase is simultaneously focusing and decelerating, in order to expect the advantages

of the active beam dump scheme, it is important to set the length of the decelerating stage in such a way that the bunch remains within this phase of the wake. The initial phase space, shown in Fig. 5(b), is the same seen in the previous simulations. Figure 5(c) shows that the propagating beam maintains its initial length until $s \simeq 1.6\,cm$. At this point, due to the phase slippage, it is close to the middle of the decelerating region, where the transverse wakefield is defocusing for the beam. Since the focusing force becomes weaker at this position, the beam radius accordingly grows, as shown in panel (c). For this propagation distance, $s \simeq 1.6\,cm$, Fig. 5(d) shows that the longitudinal phase space of the beam is still approximately flat, with some energy spread caused by the radial dependence of the longitudinal wake.

After propagating $s \simeq 2.1\,cm$, the normalized beam energy has the minimum value observed in the simulation, $U/U_0 \simeq 0.08$. At this point, Fig. 5(e) shows particles being transversely expelled at the head of the beam, which, owing to phase slippage, enters the defocusing region of the wakefield. The same panel shows that the tail of the beam is entering in the accelerating region of the wakefield due to beam lengthening. Figure 5(e) shows a phase space similar to the one observed in the 1D simulation of the active dumping scheme, the main difference being the higher energy spread due to the betatron oscillations.

In Fig. 5(g), we compare the analytical solution of the normalized total energy U/U_0 (dashed curve, black), given in Eq. (14), with the result from the 2D axi-symmetric simulation performed with INF&RNO (solid curve, blue). A good agreement between the analytical model and simulation results is observed up to a propagation distance such that the whole beam is still contained in the decelerating and focusing region ($s \lesssim 1.6\,cm$). After this, particles at the head and tail of the beam are gaining energy from the radial defocusing force and axial accelerating field, respectively. Beyond this propagation distance, the analytical solution no longer follows the behavior observed in the simulation. The modulation seen in the PIC simulation result for U/U_0 shown in Fig. 5(g) (solid curve, blue) is caused by residual mismatch oscillations of the laser pulse in the plasma channel.

At $s \simeq 2.1\,cm$, where the beam attains minimum energy, the remaining energy is dominated by particles at head and tail of the beam (nonlinear chirp). The particles at the beam's center have $U/U_0 \lesssim 0.02$, which is much lower than those at the head and tail, where $U/U_0 \simeq 0.2$. Hence, reducing the energy chirp is required to improve the beam energy extraction.

The energy chirp observed in the phase space of the beam at $s \simeq 2.1\,cm$, Fig. 5(f), can be further reduced by adjusting the initial relative phase between the beam and laser wake. For $\psi_0 = -k_pL \simeq -0.5$, at $s=0$, the beam will be within the accelerating (and focusing) phase of the laser wake, with its head aligned with the beginning of the decelerating phase (note that, for $\psi_0 = 0$, the tail of the beam was located at this position, with the whole beam contained in the decelerating phase). Then, its head (which contains the most energetic particles) will be able to propagate within the decelerating phase of the wake for a longer distance, if compared to the previous case ($\psi_0 = 0$).

In Fig. 6(a), the beam phase space obtained from the simulation with $\psi_0 = -k_pL$ (blue dots) shows a substantial reduction of high-energy particles at both head and tail of the beam, in comparison the case with $\psi_0 = 0$ (green dots). Since the tail of the beam is formed by particles that were first decelerated to non-relativistic velocities (lagging behind the faster, relativistic particles), its higher energy in the phase space comes from the propagation within the accelerating phase of the laser wake after the beam lengthening. For $\psi_0 = -k_pL$, the tail remains in this phase for a shorter distance than for $\psi_0 = 0$; this may be the cause of the energy reduction observed at the tail for $\psi_0 = -k_pL$. Each phase space is plotted at the propagation distance at which the beam total energy is minimum. This information can be obtained from the inset of panel (a), where results from PIC simulations and analytical solutions are represented with solid and dashed curves, respectively. For $\psi_0 = 0$ (green curve, solid), we observe the minimum $U/U_0 \simeq 0.08$ at $s \simeq 2.1\,cm$. For $\psi_0 = -k_pL$ (blue curve, solid), the minimum value is $U/U_0 \simeq 0.053$, observed at $s \simeq 2.5\,cm$. Figure 6(b), plotted at the same propagation distances as panel (a), shows the fraction of beam particles with energy higher than a given value of U/U_0 in the abscissa. From this panel, we see that the highest energy observed after deceleration was reduced from $U/U_0 \simeq 0.26$, for $\psi_0 = 0$ (right tail of the green filling), to $U/U_0 \simeq 0.12$, for $\psi_0 = 0$ (right tail of the blue filling). The fraction of particles with $U/U_0 > 0.10$, for example, was reduced from ~ 0.34 to ~ 0.10.

This case illustrates one of the possibilities to improve the beam energy extraction. By gradually reducing the on-axis plasma density, one could increase the dephasing length as the beam propagates. This option, along with optimizing beam loading effects and combining multiple plasma-based
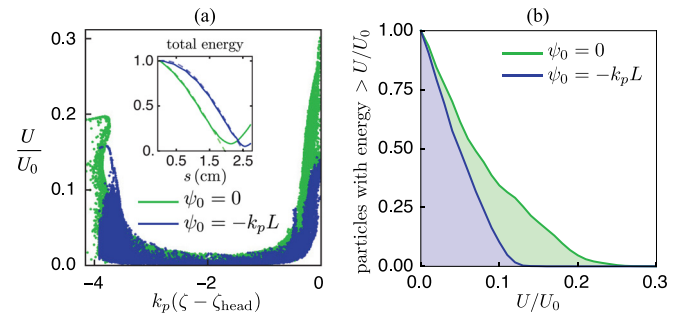

FIG. 6. Beam energy distribution after deceleration in an active beam dump, for two different values of the initial relative phase: $\psi_0 = 0$ (green dots, curves and fillings), and $\psi_0 = -k_pL \simeq -0.5$ (blue dots, curves and fillings). All other parameters are the same as Fig. 5. (a) Beam phase space, plotted at the propagation distances at which the beam total energy from each respective PIC simulation (solid curves in the inset), is minimum; (b) relative frequency of particles with energy higher than U/U_0, plotted at the same propagation distances as panel (a). For $\psi_0 = -k_pL$, although the whole beam starts the propagation in the accelerating phase of the laser wake, its head (which contains the most energetic particles) propagates within the decelerating and focusing phase for a longer distance. Then, the minimum beam total energy for $\psi_0 = -k_pL$, $U/U_0 = 0.053$, is lower than the one for $\psi_0 = 0$, $U/U_0 = 0.08$. The beam energy chirp is also reduced in the case with $\psi_0 = -k_pL$. By changing the phase from $\psi_0 = 0$ to $\psi_0 = -k_pL$, the fraction of beam particles with $U/U_0 > 0.1$, for example, is reduced from ~ 0.34 to ~ 0.10 approximately.

beam dumps, is one of the options with potential for further improvement.

V. HEATING AND RADIATION

In a plasma-based beam dump, energy from then beam is extracted and deposited into coherent plasma oscillations, and this energy will heat the plasma via collisions. It should be noted that an active plasma beam dump is similar to an LPA, but with the beam properly phased in the laser-driven wake to provide beam deceleration. In LPA experiments, the wakefield driven by the laser (with energies up to tens of joules) is larger than the wake driven by the accelerated beam, and the plasma heating caused by the laser is dominant. Therefore, in a plasma-based beam dump cooling requirements (if any) will be similar to those for acceleration in an LPA (which currently does not require a dedicated cooling system to run at $\sim$ Hz repetition rates). In addition to heating, radiation is emitted due to the betatron motion of electrons in the plasma wave.[19] However, as we show below, the energy in the betatron emission is much lower than the energy from bremsstrahlung radiation in the conventional beam dump.

Plasma-based beam dumps could be implemented using the same plasma sources adopted in current LPA experiments, i.e., gas jets or gas-filled capillaries. In a gas jet, a gas—for example, hydrogen—flowing from a nozzle in the supersonic regime (Mach of 1.2–5) can be ionized by a laser pre-pulse, which creates a $\sim$ mm-long plasma channel. A capillary consists of a hollow channel machined in a block of, for example, sapphire, typically with a circular cross section, inside which the gas is injected and confined. Electric discharges can be used to ionize the gas inside the capillary, creating a plasma channel with a parabolic density profile suitable for guiding the laser pulse over a few centimeters.[20] Due to the high-speed gas flow and the open geometry, heating in a gas jet is not as critical as in a capillary, in which the gas is confined. To investigate the plasma heating caused by a plasma-based beam dump, we shall consider the active scheme, which transfers more energy to the plasma than the passive scheme, and the use of a capillary. The plasma will receive energy from the capillary discharge (to create the plasma channel), laser (ionization and wakefield excitation), and electron beam, and the resulting heat will be dissipated in the capillary wall. For example, in the 2D axi-symmetric simulation from Sec. IV, $U/U_0 \simeq 0.053$ after deceleration, i.e., approximately $0.95 U_0 \simeq 5$ mJ would be deposited in the plasma. Note that, for a plasma with density $n_0 = 10^{18}$ cm^{-3} confined in a capillary[3] with a typical radius of $250\,\mu$m and length of 2.5 cm (at which the maximum deceleration was observed in Sec. IV), the heating due to the plasma-based beam dump would have the same order of magnitude as the heating due to the capillary discharge[20] to create a plasma channel. Due to diffraction, the disposal of the laser pulse after exiting the capillary typically is not a concern (it can be achieved by using a ceramic dump, for example). However, the energy depleted from the laser pulse along the propagation in the capillary is deposited in the plasma. In the aforementioned simulation, this corresponds to 15% of the laser

pulse energy U_l. Since $U_l \simeq \tau_t(\pi r_w^2 I_0)/2$, where τ_l is the pulse duration and I_0 is the peak laser intensity, approximately 87 mJ would be deposited in the plasma for the adopted parameters. The active beam dump would then deposit a total of $\simeq 92$ mJ in the plasma. For a repetition rate of 1 kHz, for example, an average heat of $\simeq 92$ W would be dissipated in the capillary wall. Preliminary calculations show that this could be addressed by a water-based cooling system. For a general case, the need or feasibility of a cooling system to handle the additional heat has to be analyzed taking in account the specific parameters of the beam, plasma-based beam dump, and repetition rate.

Beam deceleration in a conventional beam dump is achieved by scattering, producing radiation (bremsstrahlung photons) with a continuous spectrum that extends out to the energy of the electrons from the incident beam, $U_{max} = \gamma_0 mc^2$. The high-energy photons emitted when stopping a $\sim$ GeV beam greatly exceeds the 10–30 MeV thresholds for gamma-neutron reactions in typical shielding materials.[21,22] Muons—which are much heavier than electrons, requiring larger beam dumps to be stopped—can also be produced if the energy of the radiation is sufficiently high.[23] By adding a plasma-based deceleration stage before the conventional beam dump, the upper bound for the energy of the of bremsstrahlung radiation, U_{max}, is reduced to the highest residual energy observed in the decelerated beam. For example, in the 2D axi-symmetric simulation for an active beam dump, shown in Sec. IV, the maximum energy from the bremsstrahlung would be reduced to $U_{max} \simeq 0.16\, U_0 \simeq 80$ MeV. This energy reduction would prevent generation of muons and, even though U_{max} is still above typical thresholds for gamma-neutron reactions, since only a fraction of the beam electrons have such energy, neutrons would be produced with a significantly lower yield. For example, in the mentioned simulation, $\simeq 60\%$ of the beam particles have energy lower than 18.7 MeV, which is the gamma-neutron threshold for the carbon isotope ^{12}C.

In a plasma-based beam dump, due to the radial force in the plasma, relativistic electrons undergo transverse oscillations about the propagation axis (betatron oscillations), generating emission of synchrotron radiation. For $\sim$ GeV beams, the betatron strength parameter $a_\beta \equiv \gamma_0 k_\beta r_\beta$, where $k_\beta \simeq k_p/\sqrt{2\gamma}$ is the betatron wave number and r_β is the amplitude of the betatron orbit, typically satisfies $a_\beta \gg 1$. In this limit, a continuum of radiation is generated, that extends out to a critical frequency $\omega_{\beta,c}$, beyond which the radiation intensity diminishes. The radiation is contained in a cone about the backscatter direction, with an angle $\theta_c \lesssim a_\beta/\gamma_0$. By assuming a betatron orbit with amplitude equal to the RMS beam radius, $r_\beta = \sigma_r$, the critical frequency on axis ($\theta = 0$) is $\omega_{\beta,c} \simeq 3ck_p^2\sigma_r\gamma_0^2/2$, and the total energy radiated by the beam along the propagation in the plasma is $U_\beta/U_0 \sim \pi k_p^4 r_e \sigma_r^2 L_p \gamma_0/6$, where r_e is the electron classical radius, and L_p is the plasma length. For the set of parameters used in this paper, the energy associated with the critical frequency of the betatron radiation is $U_{\beta,c} = \hbar\omega_{\beta,c} \simeq 10$ keV, which is much lower than the maximum energy from bremsstrahlung radiation ($U_{\beta,c}/U_{max} \sim 10^{-4}$), and can be shielded effectively by

conventional beam dumps with thickness $\lesssim 1$ mm. For example, for our set of parameters, a beam with $\gamma_0 \sim 10^4$ would be required to have gamma-neutron reactions in the carbon isotope ^{12}C caused by betatron radiation. In order to have the betatron critical frequency comparable to the frequency of the bremsstrahlung radiation, a beam with $\gamma_0 \sim 2mc/(3\hbar k_p^2 \sigma_r \beta)$ would be required. For our set of parameters, this corresponds to $\gamma_0 \sim 10^7$, i.e., a beam with energy ~ 10 TeV.

VI. SUMMARY AND CONCLUSIONS

In this paper, we investigated the energy loss of relativistic electron beams undergoing passive and active plasma-based dumping schemes. An analytical model for the beam energy loss in both passive and active methods was derived. Analytical results were compared with PIC simulation results, showing good agreement.

In the passive dump scheme, the beam total energy loss is a linear function of the propagation distance only. However, due to the gradient of the wake along the beam, particles closer to the tail lose energy, while those closer to the head mostly retain their energy during the entire propagation. This causes an energy chirp (seen in the space phase of PIC simulations presented in Sec. III). Once particles closer to the tail are decelerated to non-relativistic velocities, the beam undergoes a rapid lengthening. At this point, the beam energy loss is no longer described correctly by the analytical model, which assumes a stiff beam profile. For longer propagation distances, the low-energy, non-relativistic particles in the tail of the bunch start entering the accelerating phase of the wake. From this point, the energy loss of particles toward the head of the beam is compensated by the energy gain of particles in the tail, and the integrated beam energy does not decreases anymore. For the simulations presented in Sec. III, the saturation occurs after a propagation distance of ~ 8 cm, and the minimum beam energy is around $U/U_0 \simeq 0.4$. Both 1D and 3D cases investigated in the passive dumping scheme presented similar behavior. The theoretical distance s_{max}, at which the beam would lose all its energy ($U/U_0 = 0$), is presented as an estimate of the length required to dump a given electron beam using a passive dump scheme. For fixed beam parameters, s_{max} is minimum, as expected, for a density such that $L \sim k_p^{-1}$.

In the active beam dump scheme, a laser-driven wakefield is used to generate a wakefield that provides for a more uniform beam energy extraction between head and tail, significantly reducing the observed chirp observed in the passive dump scheme. Also, since the total wakefield is larger than the one generated by the beam alone, beam energy is extracted faster with this scheme compared to the passive case. The active method also overcomes the saturation observed in the previous scheme. For example, PIC simulations in Sec. IV show more than 90% of the beam energy extracted after ~ 2 cm of propagation. After deceleration, beam total energies of $U/U_0 \simeq 0.03$ and $U/U_0 \simeq 0.08$ were observed for 1D and 2D axi-symmetric simulations, respectively. By properly selecting the initial relative phase between laser and beam, the minimum beam total energy was lowered to $U/U_0 \simeq 0.053$, with a reduced beam energy chirp.

Other parameters can be adjusted to improve the energy extraction and reduce the energy chirping. Reducing the on-axis plasma density, tailoring the longitudinal plasma density profile, and optimizing the phasing/beam loading effects are some of the options for optimization. Plasma-based beam dumps are a promising method to decelerate electron beams with $\sim$ GeV energies over centimeter-scale distances, since they could reduce the size of conventional dumping structures and emission of secondary particles (lowering the yield of neutrons and mostly eliminating the production of muons). These schemes could be used to improve the overall compactness of LPAs, making them more suitable for portable applications such as quasi-monoenergetic light sources from Thomson scattering.[10] For these energies, the additional heat transferred from the beam to the plasma would not be an issue for repetition rates up to $\sim$ kHz. The amount of energy that can be extracted from an electron beam by using the active dump method is limited by the dephasing length and by laser energy depletion. In order to fully deplete the energy of a beam with an arbitrarily high initial energy, it may be necessary to improve the energy extraction by using the aforementioned options, and/or to work with multiple active beam dump stages. These options will be investigated in a forthcoming paper.

[1] E. Esarey, P. Sprangle, J. Krall, and A. Ting, Plasma Sci. **24**, 252 (1996).
[2] E. Esarey, C. B. Schroeder, and W. P. Leemans, Rev. Mod. Phys. **81**, 1229 (2009).
[3] W. P. Leemans, A. J. Gonsalves, H. S. Mao, K. Nakamura, C. Benedetti, C. B. Schroeder, C. Toth, J. Daniels, D. E. Mittelberger, S. S. Bulanov, J. L. Vay, C. G. R. Geddes, and E. Esarey, Phys. Rev. Lett. **113**, 245002 (2014).
[4] P. Chen, J. M. Dawson, R. W. Huff, and T. Katsouleas, Phys. Rev. Lett. **54**, 693 (1985).
[5] J. B. Rosenzweig, D. B. Cline, B. Cole, H. Figueroa, W. Gai, R. Konecny, J. Norem, P. Schoessow, and J. Simpson, Phys. Rev. Lett. **61**, 98 (1988).
[6] M. Litos, E. Adli, W. An, C. I. Clarke, C. E. Clayton *et al.*, Nature **515**, 92 (2014).
[7] H. C. Wu, T. Tajima, D. Habs, A. W. Chao, and J. Meyer-ter Vehn, Phys. Rev. Spec. Top. Accel. Beams **13**, 101303 (2010).
[8] R. Lehe, C. Thaury, E. Guillaume, A. Lifschitz, and V. Malka, Phys. Rev. Spec. Top.-Accel. Beams **17**, 121301 (2014).
[9] J.-L. Vay, C. G. R. Geddes, S. G. Rykovanov, C. B. Schroeder, E. Esarey, and W. P. Leemans, in Proceedings of the Nuclear Physics and Gamma-Ray Sources for Nuclear Security and Nonproliferation—NPNSNP (World Scientific, 2015).
[10] S. G. Rykovanov, C. G. R. Geddes, J. L. Vay, C. B. Schroeder, E. Esarey, and W. P. Leemans, J. Phys. B: At., Mol. Opt. Phys. **47**, 234013 (2014).
[11] R. Keinigs and M. E. Jones, Phys. Fluids **30**, 252 (1987).

[12]C. Benedetti, C. B. Schroeder, E. Esarey, and W. P. Leemans, Phys. Plasmas **19**, 053101 (2012).

[13]A. Bonatto, C. B. Schroeder, J. L. Vay, C. G. R. Geddes, C. Benedetti, E. Esarey, and W. P. Leemans, in Proceedings of the 2014 AAC Workshop (2014).

[14]J.-L. Vay, D. P. Grote, R. H. Cohen, and A. Friedman, Comput. Sci. Discovery **5**, 014019 (2012).

[15]J. L. Vay, Phys. Rev. Lett. **98**, 130405 (2007).

[16]C. Benedetti, F. Rossi, E. Esarey, C. B. Schroeder, and W. P. Leemans, Phys. Rev. E (submitted).

[17]C. Benedetti, C. B. Schroeder, E. Esarey, C. G. R. Geddes, and W. P. Leemans, in *Proceedings of the 2010 AAC Workshop* (2010), Vol. 1299, p. 250.

[18]C. Benedetti, C. B. Schroeder, E. Esarey, and W. P. Leemans, in *Proceedings of the ICAP 2012* (2012), p. 206.

[19]E. Esarey, B. Shadwick, P. Catravas, and W. P. Leemans, Phys. Rev. E **65**, 056505 (2002).

[20]N. A. Bobrova, A. A. Esaulov, J. I. Sakai, P. V. Sasorov, D. J. Spence, A. Butler, S. M. Hooker, and S. V. Bulanov, Phys. Rev. E **65**, 016407 (2001).

[21]W. P. Leemans, D. Rodgers, P. E. Catravas, C. G. R. Geddes, G. Fubiani, E. Esarey, B. A. Shadwick, R. Donahue, and A. Smith, Phys. Plasmas **8**, 2510 (2001).

[22]R. B. Firestone, V. S. Shirley, C. M. Baglin, and S. Chu, *Table of Isotopes*, 8th ed. (John Wiley & Sons, New York, 1996).

[23]K. A. Olive *et al.* (Particle Data Group), Chin. Phys. C **38**(9), 090001 (2014).